CrossMark

Potential Singularity for a Family of Models of the Axisymmetric Incompressible Flow

Thomas Y. Hou[1] · Tianling Jin[2] · Pengfei Liu[1]

Abstract We study a family of 3D models for the incompressible axisymmetric Euler and Navier–Stokes equations. The models are derived by changing the strength of the convection terms in the equations written using a set of transformed variables. The models share several regularity results with the Euler and Navier–Stokes equations, including an energy identity, the conservation of a modified circulation quantity, the BKM criterion and the Prodi–Serrin criterion. The inviscid models with weak convection are numerically observed to develop stable self-similar singularity with the singular region traveling along the symmetric axis, and such singularity scenario does not seem to persist for strong convection.

Keywords Self-similar singularity · Axisymmetric incompressible flow · Stabilizing effect of convection

Mathematics Subject Classification 35Q31

Communicated by Alex Kiselev.

✉ Pengfei Liu
plliu@caltech.edu

Thomas Y. Hou
hou@cms.caltech.edu

Tianling Jin
tianlingjin@ust.hk

[1] Applied and Computational Mathematics, California Institute of Technology, Pasadena, CA 91125, USA

[2] Department of Mathematics, The Hong Kong University of Science and Technology, Clear Water Bay, Kowloon, Hong Kong

1 Introduction

The 3D incompressible Euler and Navier–Stokes equations govern the motion of ideal incompressible fluid and take the following simple form

$$\mathbf{u}_t + \mathbf{u} \cdot \nabla \mathbf{u} = -\nabla p + \nu \Delta \mathbf{u}, \quad \nabla \cdot \mathbf{u} = 0, \tag{1.1}$$

where $\mathbf{u}(x, t) : R^3 \times [0, T) \to R^3$ describes the 3D velocity field of the fluid, and $p(x, t) : R^3 \times [0, T) \to R$ describes the pressure in the fluid. The divergence-free condition $\nabla \cdot \mathbf{u} = 0$ guarantees the incompressibility of the fluid. The Laplace term $\nu \Delta \mathbf{u}$ models the viscosity in the fluid; for inviscid fluid with $\nu = 0$, Eq. (1.1) are called the Euler equations, and for the viscous case $\nu > 0$, Eq. (1.1) are called the Navier–Stokes equations. The 3D Euler and Navier–Stokes equations are among the most fundamental nonlinear PDEs in nature yet far from being fully understood. The fundamental question regarding the global regularity of the 3D Euler and Navier–Stokes equations with smooth initial data remains open and is viewed as one of the most important open questions in mathematical fluid mechanics; see Fefferman (2006).

The Euler and Navier–Stokes equation (1.1) enjoy the energy identity,

$$\frac{1}{2} \|\mathbf{u}(x, t)\|_{L^2(R^3)}^2 + \nu \int_0^t \|\nabla \mathbf{u}(x, s)\|_{L^2(R^3)}^2 = \frac{1}{2} \|\mathbf{u}(x, 0)\|_{L^2(R^3)}^2, \tag{1.2}$$

where $\frac{1}{2} \int_{R^3} |\mathbf{u}(x, t)|^2 \mathrm{d}x$ and $\nu \int_0^T \int_{R^3} |\nabla \mathbf{u}(x, t)|^2 \mathrm{d}x \mathrm{d}t$ seem to be the only known coercive *a priori* estimates of smooth solutions to (1.1). The difficulty for the global regularity of the Navier–Stokes equations lies in the fact that these known *a priori* estimates are supercritical with respect to the invariant scaling of the equations; see Tao (2008) for more about this supercritical barrier. For the Euler equations, due to the lack of regularization mechanism, to establish global regularity of the solutions becomes even more challenging.

In this work, we investigate a family of 3D models for the 3D Euler and Navier–Stokes equations with axial symmetry. The family of models are derived by changing the strength of the convection terms in the equations written using a set of transformed variables, $u_1 = \frac{u^\theta}{r}$, $\omega_1 = \frac{\omega^\theta}{r}$, where u^θ and ω^θ are the angular components of the velocity and vorticity fields, respectively. The family of 3D models can be written in terms of u_1 and ω_1 as follows,

$$u_{1,t} + u^r u_{1,r} + u^z u_{1,z} = \nu \left(\partial_r^2 + \frac{3}{r} \partial_r + \partial_z^2 \right) u_1 + 2u_1 \phi_{1,z},$$

$$\omega_{1,t} + u^r \omega_{1,r} + u^z \omega_{1,z} = \nu \left(\partial_r^2 + \frac{3}{r} \partial_r + \partial_z^2 \right) \omega_1 + \left(u_1^2 \right)_z,$$

$$-\left[\partial_r^2 + (3/r)\partial_r + \partial_z^2 \right] \phi_1 = \omega_1,$$

with the Biot–Savart law given by

$$u^r = -\epsilon r \phi_{1,z}, \quad u^z = \epsilon (2\phi_1 + r\phi_{1,r}).$$

The parameter ϵ is used to control the strength of the convection terms. The case $\epsilon = 1$ corresponds to the original axisymmetric Euler and Navier–Stokes equations, and the case $\epsilon = 0$ corresponds to the 3D model proposed by Hou and Lei (2009). It has been numerically shown in Hou and Lei (2009) and Hou et al. (2012, 2014) that the above inviscid model with $\epsilon = 0$ can develop potential finite-time singularity.

In this work, we study the above 3D models with the parameter $\epsilon \in [0, 2)$ to demonstrate the subtle balance between the nonlinear convection and the nonlinear vortex stretching. Our study shows that the competition between the convection and the vortex stretching may be responsible for the potential singularity formation or depletion of nonlinearity of the equations.

The family of models share several regularity results with the Euler and Navier–Stokes equations, including an energy identity, the conservation of a modified circulation quantity, a BKM-type criterion for the inviscid model, and a Prodi–Serrin type criterion for the viscous model. The energy functional for the models is equivalent to that of the original Euler and Navier–Stokes equations. We derive an equivalent formulation of the models written in the velocity–pressure formulation, and they can be viewed as the original Eq. (1.1) with an added stirring forcing term. To control this additional term in our proof of the regularity criteria, we need to use some estimates for the Sobolev norms of axisymmetric solenoidal vector fields.

Despite the similarities between the proposed models and the original Euler equations, the inviscid models demonstrate very different regularity properties based on our numerical computation. Our numerical results suggest that for weak convection, the inviscid models develop finite-time singularity with local self-similar structure, and the singular region is not stationary but traveling along the symmetric axis. To resolve the singular numerical solutions, we employ an adaptive moving mesh method proposed in Luo and Hou (2014), which adaptively puts a certain portion of the grid points in the singular region of the solutions. We numerically observe that as we increase the strength of the convection terms, such singularity scenario is destroyed. Specifically, this singularity scenario does not seem to persist for the original Euler equations.

We also employ a dynamic rescaling formulation to demonstrate the stability of the self-similar singularity. In the dynamic rescaling formulation, we add scaling and shifting terms to the models according to the scaling and translational invariance properties of the equations, and the resulting equations govern the evolution of the spatial profiles in the original solutions. The self-similar profiles in the singular solutions correspond to the steady state of the dynamic rescaling equations, and we demonstrate the stability of the self-similar profiles by linearizing the discretized dynamic rescaling equations at the steady state. We observe that for weak convection, the real parts of the eigenvalues of the Jacobian matrix are all negative, which demonstrates the linear stability of the traveling wave self-similar singularity scenario. However, as the strength of the convection increases, the dominating eigenvalues of the Jacobian matrix with the largest real parts seem to approach the imaginary axis. This implies that the steady state of the dynamic rescaling equations becomes less stable as the strength of the convection increases.

The rest of the paper is organized as follows. In Sect. 2, we derive the models and give a brief review of some of the previous works on the regularity of the 3D Euler and Navier–Stokes equations. In Sect. 3, we prove some regularity results for

the family of models, including some conserved quantities and non-blow-up criteria. In Sect. 4, we solve the inviscid models numerically and present some features of the finite-time singularity. We also present stability results for the self-similar singularity of the inviscid models using the dynamic rescaling formulation. Concluding remarks are made in Sect. 5.

2 Derivation of the Models and Review of Previous Works

In this section, we derive the models and give a brief review of some of the previous works for 3D Euler and Navier–Stokes equations.

2.1 Derivation of the Models

Let $\mathbf{e_r}, \mathbf{e}_\theta$ and $\mathbf{e_z}$ be the standard orthonormal vectors defining the cylindrical coordinate system,

$$\mathbf{e_r} = \left(\frac{x_1}{r}, \frac{x_2}{r}, 0\right)^T, \quad \mathbf{e}_\theta = \left(\frac{x_2}{r}, -\frac{x_1}{r}, 0\right)^T, \quad \mathbf{e_z} = (0, 0, 1)^T,$$

where $r = \sqrt{x_1^2 + x_2^2}$ and $z = x_3$. Then the 3D velocity field $\mathbf{u}(x, t)$ is called axisymmetric if it can be written as

$$\mathbf{u} = u^r(r, z, t)\mathbf{e_r} + u^\theta(r, z, t)\mathbf{e}_\theta + u^z(r, z, t)\mathbf{e_z},$$

where u^r, u^θ and u^z do not depend on the θ coordinate.

The Euler and Navier–Stokes equations with axisymmetric velocity field can be written in the cylindrical coordinates as

$$u_t^\theta + u^r u_r^\theta + u^z u_z^\theta = \nu \left(\Delta - \frac{1}{r^2}\right) u^\theta - \frac{u^r u^\theta}{r}, \tag{2.1a}$$

$$\omega_t^\theta + u^r \omega_r^\theta + u^z \omega_z^\theta = \nu \left(\Delta - \frac{1}{r^2}\right) \omega^\theta + \frac{2}{r} u^\theta u_z^\theta + \frac{u^r \omega^\theta}{r}, \tag{2.1b}$$

$$-\left[\Delta - \frac{1}{r^2}\right] \phi^\theta = \omega^\theta, \tag{2.1c}$$

where the radial and angular velocity fields u^r and u^θ are recovered from ϕ^θ based on the Biot–Savart law

$$u^r = -\partial_z \phi^\theta, \quad u^z = r^{-1} \partial_r (r\phi^\theta). \tag{2.2}$$

Note that Eqs. (2.1–2.2) have a formal singularity on the axis $r = 0$ due to the $\frac{1}{r}$ terms. Because the angular components $u^\theta(r, z)$, $\omega^\theta(r, z)$ and $\phi^\theta(r, z)$ can all be viewed as odd functions of r (Liu and Wang 2006), one can introduce the following transformed variables (Hou and Li 2008) to remove the formal singularity in (2.1),

$$u_1 = u^\theta/r, \quad \omega_1 = \omega^\theta/r, \quad \phi_1 = \phi^\theta/r. \tag{2.3}$$

Then one can get the equations for u_1 and ω_1 as the following:

$$u_{1,t} + u^r u_{1,r} + u^z u_{1,z} = \nu\left(\partial_r^2 + \frac{3}{r}\partial_r + \partial_z^2\right)u_1 + 2u_1\phi_{1,z}, \tag{2.4a}$$

$$\omega_{1,t} + u^r \omega_{1,r} + u^z \omega_{1,z} = \nu\left(\partial_r^2 + \frac{3}{r}\partial_r + \partial_z^2\right)\omega_1 + (u_1^2)_z, \tag{2.4b}$$

$$-\left[\partial_r^2 + (3/r)\partial_r + \partial_z^2\right]\phi_1 = \omega_1, \tag{2.4c}$$

with the Biot–Savart law given by

$$u^r = -r\phi_{1,z}, \quad u^z = 2\phi_1 + r\phi_{1,r}. \tag{2.5}$$

For axisymmetric flow, the incompressibility condition becomes

$$\partial_r(ru^r) + \partial_z(ru^z) = 0. \tag{2.6}$$

The Euler and Navier–Stokes equations with axial symmetry have an additional conserved quantity besides the energy (1.2). The total circulation $\Gamma = ru^\theta = r^2u_1$ satisfies the maximum principle,

$$\partial_t\Gamma + u^r\Gamma_r + u^z\Gamma_z = \nu\left(\Delta - \frac{2}{r}\partial_r\right)\Gamma, \quad \|\Gamma(\cdot,t)\|_{L^\infty} \le \|\Gamma(\cdot,0)\|_{L^\infty}. \tag{2.7}$$

We change the strength of the convection terms in the Euler and Navier–Stokes equation (2.4) by a factor of ϵ and get the following Biot–Savart law and models of the Euler and Navier–Stokes equations,

$$u^r = -\epsilon r\phi_{1,z}, \quad u^z = 2\epsilon\phi_1 + \epsilon r\phi_{1,r}. \tag{2.8}$$

In this work, we study the family of models (2.8) with $\epsilon \in [0, 2)$ to demonstrate the balance between the convection terms and the vortex stretching terms in (2.4), and the potential stabilizing effect of convection.

Note that we change the strength of the convection in a form of the Euler and Navier–Stokes equations written using transformed variables u_1 and ω_1 (2.3), not the original velocity–pressure form (1.1). Next we derive an equivalent formulation for the family of models (2.8) in the velocity–pressure formulation.

Multiplying Eq. (2.4) by r and using (2.8), we get

$$u_t^\theta + u^r u_r^\theta + u^z u_z^\theta - \frac{u^r u^\theta}{r} = -\frac{2}{\epsilon}\frac{u^r u^\theta}{r} + \nu\left(\Delta - \frac{1}{r^2}\right)u^\theta, \tag{2.9}$$

$$\omega_t^\theta + u^r \omega_r + u^z \omega_z - \frac{u^r \omega^\theta}{r} = \frac{(u^\theta)_z^2}{r} + \nu\left(\Delta - \frac{1}{r^2}\right)\omega^\theta. \tag{2.10}$$

Because the $\frac{1}{\epsilon}$ term does not allow $\epsilon = 0$, we make change of variables

$$v^r = \frac{u^r}{\epsilon} = -r\phi_{1,z}, \quad v^z = \frac{u^z}{\epsilon} = 2\phi_1 + r\phi_{1,r}, \quad v^\theta = \frac{u^\theta}{\epsilon^{3/2}}. \tag{2.11}$$

Based on (2.8) and (2.4c), we have

$$\omega^\theta = (\partial_z v^r - \partial_r v^z). \tag{2.12}$$

Then we denote $F_r(t, r, z)$ and $F_z(t, r, z)$ as

$$F_r(t, r, z) = v_t^r + \epsilon v^r v_r^r + \epsilon v^z v_z^r - \epsilon \frac{(v^\theta)^2}{r} - v \left(\Delta - \frac{1}{r^2} \right) v^r,$$

$$F_z(t, r, z) = v_t^z + \epsilon v^r v_r^z + \epsilon v^z v_r^z - v \Delta v^z.$$

Comparing $\partial_z F^r - \partial_r F^z$ with (2.10), we obtain

$$\partial_z F^r(t, r, z) - \partial_r F^z(t, r, z) = 0,$$

so there exists a scalar field p such that $F^r = \partial_z p$, $F^z = \partial_r p$. Namely,

$$v_t^r + \epsilon v^r v_r^r + \epsilon v^z v_z^r - \epsilon \frac{(v^\theta)^2}{r} + \partial_r p = v \left(\Delta - \frac{1}{r^2} \right) v^r, \tag{2.13}$$

$$v_t^z + \epsilon v^r v_r^z + \epsilon v^z v_r^z + \partial_z p = v \Delta v^z. \tag{2.14}$$

And p is determined by the incompressibility condition (2.6).

Then we denote the new velocity field $\mathbf{v}$ as

$$\mathbf{v} = v^r \mathbf{e_r} + v^\theta \mathbf{e}_\theta + v^z \mathbf{e_z}.$$

Changing Eqs. (2.13), (2.14) back to the physical coordinates, we get

$$\mathbf{v}_t + \epsilon \mathbf{v} \cdot \nabla \mathbf{v} = -\nabla p + v \Delta \mathbf{v} + (2\epsilon - 2) \frac{v^\theta v^r \mathbf{e}_\theta}{r}. \tag{2.15}$$

So the family of models, (2.4) and (2.8), which are originally derived by changing the strength of the convection terms in the governing equations of a set of transformed variables $\frac{u^\theta}{r}$ and $\frac{\omega^\theta}{r}$, can also be derived by changing the strength of convection in (1.1) and adding a stirring forcing of the form

$$\mathbf{F} = (2\epsilon - 2) \frac{v^\theta v^r \mathbf{e}_\theta}{r}.$$

Remark 2.1 The third change of variable in (2.11) requires $\epsilon > 0$, without which we will get an additional radial forcing term $\frac{(v^\theta)^2}{r} \mathbf{e_r}$ in (2.15), and our proof of the regularity results in Sect. 3 still goes through.

2.2 Review of Regularity Results for the 3D Euler and Navier–Stokes Equations

A lot of important progresses have been made concerning the regularity of the Euler and Navier–Stokes equations. In the 2D case, the global regularity holds (Majda and Bertozzi 2002) because one can get *a priori* estimate of the maximum vorticity $\omega = \nabla \times \mathbf{u}$. For the Euler equations, the celebrated BKM criterion (Beale et al. 1984; Ferrari 1993) asserts that if $\int_0^T \|\omega(t)\|_\infty dt < +\infty$, then the solutions remain smooth up to time T. We will prove the same criterion for the inviscid model (2.8) in Sect. 3. The non-blow-up criterion of Constantin et al. (1996) focuses on the geometric aspects the 3D Euler flows and asserts that there can be no blowup if the velocity field $\mathbf{u}$ is uniformly bounded and the vorticity direction $\xi = \omega/|\omega|$ is sufficiently "well behaved" near the point of maximum vorticity. The theorem of Deng et al. (2005, 2006) is similar in spirit to the Constantin–Fefferman–Majda criterion, but confines the analysis to localized vortex line segments. They assert that if the vorticity direction is well behaved on a local region near the maximum vorticity, then the solutions remain regular. To be specific, their theorems allow the area of the region to collapse to zero.

For the 3D Navier–Stokes equations, if the initial data are small in certain critical norm, say $\|\mathbf{u}\|_{L^2}\|\nabla\mathbf{u}\|_{L^2}$, then the solutions will remain bounded and smooth for all time. See Koch and Tataru (2001) for an essentially optimal result in this direction. The criterion of Prodi (1959) and Serrin (1963) claims that for $\frac{3}{p} + \frac{2}{q} = 1, 3 < p \leq +\infty$, if $\|\mathbf{u}(x, t)\|_{L^q(L^p(R^3), [0, T))} < +\infty$, then the solutions can be extended smoothly beyond time T. The critical case of $p = 3$ and $q = +\infty$ also implies regularity of the solutions, and this result was proved by Escauriaza et al. (2003) using essentially different techniques, which rely on a unique continuation property for the backward heat equations. We will prove a Prodi–Serrin type criterion for the viscous model (2.8) in Sect. 3.

To demonstrate the supercritical barrier in the 3D Navier–Stokes equations, Tao recently proposed a 3D model (Tao 2016) where the nonlinearity term $B(\mathbf{u}, \mathbf{u})$ in (1.1) is replaced by a highly non-trivial averaging term $\tilde{B}(\mathbf{u}, \mathbf{u})$. The averaged bilinear operator $\tilde{B}(\cdot, \cdot)$ shares several estimates with $B(\cdot, \cdot)$, and it is proved that the averaged model can develop finite-time singularity.

There also exist a lot of works in the literature that focus on the numerical search of a finite-time singularity for the Euler equations. See Grauer and Sideris (1991), Pumir and Siggia (1992) and Weinan and Shu (1994) for the numerical study of the axisymmetric Euler equations, and Kerr (1993), Hou and Li (2006) for Euler flows generated by perturbed antiparallel vortex tubes. The numerical results mentioned above have been non-conclusive since there is no stable structure in the potentially singular solutions. In a recent numerical computation by Luo and Hou (2014) for the 3D axisymmetric Euler equations, the solutions were observed to develop singularity on the boundary with local self-similar structure. Several works were motivated by this computation, including two 1D models (Hou and Luo 2013; Choi et al. 2014, 2015) and a self-similar singularity result (Hou and Liu 2015) for one of the models. For the inviscid models that we study in this work, the singular solutions also develop stable local self-similar structure, and the singular region is not stationary but traveling along the symmetric axis.

3 Some Regularity Results

The velocity field **v** in Eq. (2.15) is divergence-free according to (2.6),

$$\partial_r(rv^r) + \partial_z(rv^z) = \partial_r(-r^2\phi_{1,z}) + \partial_z(2r\phi_1 + r^2\phi_{1,r}) = 0,$$

and thus the 3D models (2.15) are still incompressible.

The inviscid models (2.8) with $\nu = 0$ enjoy the following scaling invariance,

$$u_1(r,z,t) \to \frac{1}{\tau}u_1\left(\frac{r}{\lambda}, \frac{z}{\lambda}, \frac{t}{\tau}\right), \quad \omega_1(r,z,t) \to \frac{1}{\lambda\tau}\omega_1\left(\frac{r}{\lambda}, \frac{z}{\lambda}, \frac{t}{\tau}\right); \quad (3.1)$$

while for the viscous models $\nu > 0$, we have,

$$u_1(r,z,t) \to \frac{1}{\tau}u_1\left(\frac{r}{\tau^{1/2}}, \frac{z}{\tau^{1/2}}, \frac{t}{\tau}\right),$$
$$\omega_1(r,z,t) \to \tau^{-3/2}\omega_1\left(\frac{r}{\tau^{1/2}}, \frac{z}{\tau^{1/2}}, \frac{t}{\tau}\right). \quad (3.2)$$

Note that the introduction of viscosity $\nu > 0$ restricts the two-parameter symmetry group in (3.1) to the one-parameter group in (3.2).

The models also enjoy translational invariance in the axial direction,

$$u_1(r,z,t) \to u_1(r, z-c, t), \quad \omega_1(r,z,t) \to \omega_1(r, z-c, t). \quad (3.3)$$

The scaling and translational invariances (3.1), (3.3) allow for the traveling self-similar singularity of the inviscid models that will be demonstrated in Sect. 4.

The Laplace operators in the evolution equations of u_1 (2.4a), ω_1 (2.4b), and the Biot–Savart law (2.4c), namely

$$\partial_r^2 + \frac{3}{r}\partial_r + \partial_z^2$$

are essentially five-dimensional Laplace operator with axial symmetry. It is convenient to view the 3D model (2.8) as defined on $y \in R^5$ with

$$y = (y_1, y_2, y_3, y_4, z) \in R^5, \quad r = \left(y_1^2 + y_2^2 + y_3^2 + y_4^2\right)^{1/2},$$

and the solutions are symmetric with respect to y_i, $i = 1, 2 \ldots 4$.

The new 3D models (2.8) enjoy the following energy identity for $\epsilon < 2$.

Theorem 3.1 *For smooth solutions to the 3D model (2.8) with $\epsilon < 2$, the following identity holds,*

$$\frac{1}{2}\frac{d}{dt}\int_{-\infty}^{\infty}\int_0^{\infty}\left(|u_1|^2 + (2-\epsilon)|\nabla_y\phi_1|^2\right)r^3 drdz$$

$$+\nu\int_{-\infty}^{\infty}\int_0^{\infty}\left(|\nabla_y u_1|^2 + (2-\epsilon)|\Delta_y\phi_1|^2\right)r^3 drdz = 0. \qquad (3.4)$$

Remark 3.2 We denote the energy functional in the above identity as,

$$E_\epsilon = \int_{-\infty}^{\infty}\int_0^{\infty}\left(|u_1|^2 + (2-\epsilon)|\nabla_y\phi_1|^2\right)r^3 drdz. \qquad (3.5)$$

For $\epsilon = 1$, E_1 is the same as the L^2 energy of the original Euler and Navier–Stokes equations in the energy identity (1.2),

$$E_1 = \frac{1}{2\pi}\int_{R^3}|\mathbf{u}|^2 dx.$$

For $\epsilon < 2$, E_ϵ is equivalent to the L^2 energy of Euler and Navier–Stokes equations. To be specific, we have that

$$\min(1, 2-\epsilon)E_1 \le E_\epsilon \le \max(1, 2-\epsilon)E_1.$$

Proof Multiplying the first Eq. (2.4a) by $u_1 r^3$, and integrating over $drdz$, which is equivalent to the 5D Lebesgue measure dy, we get

$$\frac{1}{2}\frac{d}{dt}\int u_1^2 r^3 drdz + \frac{1}{2}\int (u^r r)r^2 \left(u_1^2\right)_r drdz + \frac{1}{2}\int (u^z r)r^2 \left(u_1^2\right)_z drdz$$

$$= \int 2u_1^2\phi_{1,z}r^3 drdz - \nu\int |\nabla_y u_1|^2 r^3 drdz.$$

For the convection terms, using integration by part, one can get

$$\frac{1}{2}\int (u^r r)r^2 \left(u_1^2\right)_r drdz + \frac{1}{2}\int (u^z r)r^2 \left(u_1^2\right)_z drdz =$$

$$-\frac{1}{2}\int \left((u^r r)_r + (u^z r)_z\right)r^2 u_1^2 drdz - \int u^r r^2 u_1^2 drdz.$$

Using the divergence-free condition $(ru^r)_r + (ru^z)_z = 0$, one can get

$$\frac{1}{2}\int (u^r r)r^2 \left(u_1^2\right)_r drdz + \frac{1}{2}\int (u^z r)r^2 \left(u_1^2\right)_z drdz = -\int u^r r^2 u_1^2 drdz.$$

Then we have

$$\frac{1}{2}\frac{d}{dt}\int u_1^2 r^3 drdz - \int u^r r^2 u_1^2 drdz = \int 2u_1^2\phi_{1,z}r^3 drdz - \nu\int |\nabla_y u_1|^2 r^3 drdz.$$

Using the Biot–Savart law $u^r = -\epsilon r\phi_{1,z}$, we get that

$$\frac{1}{2}\frac{d}{dt}\int u_1^2 r^3 drdz = \int (2-\epsilon)u_1^2 \phi_{1,z} r^3 drdz - \nu \int |\nabla_y u_1|^2 r^3 drdz. \quad (3.6)$$

Multiplying (2.4b) by $\phi_1 r^3$, and using $-\Delta\phi_1 = \omega_1$, we have

$$\frac{1}{2}\frac{d}{dt}\int |\nabla\phi_1|^2 r^3 drdz + \int (u^r r)\omega_{1,r}\phi_1 r^2 drdz + \int (u^z r)\omega_{1,z}\phi_1 r^2 drdz$$
$$= -\int u_1^2 \phi_{1,z} r^3 drdz - \nu \int |\Delta_y\phi_1|^2 r^3 drdz.$$

For the convection terms, using integration by part we get

$$\int (u^r r)\omega_{1,r}\phi_1 r^2 drdz + \int (u^z r)\omega_{1,z}\phi_1 r^2 drdz =$$
$$-\int \left((u^r r)_r + (u^z r)_z\right)\omega_1\phi_1 r^2 drdz$$
$$-\int \left[u^r r\omega_1\left(\phi_1 r^2\right)_r + u^z r\omega_1\left(\phi_1 r^2\right)_z\right] drdz.$$

The first term in the RHS vanishes due to (2.6), and the second term also vanishes based on the Biot–Savart law (2.8). Then we have

$$\frac{1}{2}\frac{d}{dt}\int |\nabla\phi_1|^2 r^3 drdz = -\int u_1^2 \phi_{1,z} r^3 drdz - \nu \int |\Delta_y\phi_1|^2 r^3 drdz. \quad (3.7)$$

Adding up (3.6) and (3.7), we can complete the proof. $\square$

For the family of 3D models (2.8) with $\epsilon > 0$, we define the modified circulation as

$$\Gamma^\epsilon = r^{2/\epsilon} u_1, \quad (3.8)$$

which plays the same role as the circulation Γ for the axisymmetric Euler and Navier–Stokes equations in (2.7). We can derive the equation of Γ^ϵ as

$$\partial_t \Gamma^\epsilon + u^r \Gamma_r^\epsilon + u^z \Gamma_z^\epsilon = \nu \left(\Delta - \frac{2}{r}\left(\frac{2}{\epsilon} - 1\right)\partial_r + \frac{1}{r^2}\frac{2}{\epsilon}\left(\frac{2}{\epsilon} - 2\right)\right)\Gamma^\epsilon. \quad (3.9)$$

Then for the inviscid model with $\nu = 0$, or the viscous model with $\nu > 0$, $\epsilon \geq 1$, we have the maximal principle

$$\|\Gamma^\epsilon(r, z, t)\|_{L^\infty} \leq \|\Gamma^\epsilon(r, z, 0)\|_{L^\infty}.$$

And in the viscous models with $\epsilon > 1$, the quantity Γ^ϵ is indeed subcritical with respect to the scaling of the equations in (3.2).

For the inviscid 3D model (2.8) with $\nu = 0$, we have the following Beale–Kato–Majda type non-blow-up criterion for $\mathbf{v} = v^r \mathbf{e_r} + v^z \mathbf{e_z} + v^\theta \mathbf{e_\theta}$.

Theorem 3.3 *For initial data* $\mathbf{v}(x, 0) \in H^4(R^3)$, *if*

$$\int_0^T \|\nabla \times \mathbf{v}(t)\|_{\mathrm{BMO}} dt < +\infty, \tag{3.10}$$

then $\mathbf{v}(x, T) \in H^4(R^3)$, *and the solutions can be extended beyond time* T.

We need the following estimate proved by Kozono and Taniuchi (2000). For divergence-free velocity field $\mathbf{v}(x)$ in R^3, the following holds:

$$\|\nabla_x \mathbf{v}\|_{L^\infty} \leq C \left[1 + \|\nabla \times \mathbf{v}\|_{\mathrm{BMO}} \ln \left(1 + \|\mathbf{v}\|_{H^4}^2 \right) \right]. \tag{3.11}$$

We also need the following estimates of Klainerman and Majda (1981):

$$\|fg\|_{H^m} \leq c\|f\|_{L^\infty} \|D^m g\|_{L^2(R^N)} + c\|D^m f\|_{L^2(R^N)} \|g\|_{L^\infty}, \tag{3.12}$$

$$\sum_{0 \leq |\alpha| \leq m} \|D^\alpha (fg) - f D^\alpha g\|_{L^2(R^N)}$$
$$\leq c\|\nabla f\|_{L^\infty} \|D^{m-1} g\|_{L^2(R^N)} + c\|D^m f\|_{L^2(R^N)} \|g\|_{L^\infty}. \tag{3.13}$$

To estimate the stirring term in (2.15), we use the following Lemma.

Lemma 3.4 *For smooth axisymmetric solutions to (2.15),* $\mathbf{v} \in H^4(R^3)$,

$$\left\| D^4 \frac{v^r v^\theta \mathbf{e}_\theta}{r} \right\|_{L^2(R^3)} \leq \|\nabla \mathbf{v}\|_{L^\infty} \|\mathbf{v}\|_{H^4}.$$

We prove Lemma 3.4 using the estimates for axisymmetric solenoidal vector fields that are obtained in Liu and Wang (2006). Denote the operator $\mathcal{L}$ as

$$\mathcal{L} = -\Delta_3 + \frac{1}{r^2},$$

where Δ_3 is the three-dimensional Laplace operator

$$\Delta_3 = \partial_r^2 + \frac{1}{r}\partial_r + \partial_z^2.$$

Then for every smooth axisymmetric solenoidal vector field

$$\mathbf{F} = F^\theta \mathbf{e}_\theta - \partial_z \varphi^\theta \mathbf{e_r} + \frac{\partial_r (r\varphi^\theta)}{r} \mathbf{e_z}, \tag{3.14a}$$

we have

$$\|D^4\mathbf{F}\|^2_{L^2(R^3)} = \|\mathcal{L}^2 F^\theta\|^2_{L^2(R^3)} + \|\mathcal{L}^2\varphi^\theta\|^2_*, \tag{3.14b}$$

where

$$\|f\|^2_* = \|\partial_r f\|^2_{L^2(R^3)} + \|\partial_z f\|^2_{L^2(R^3)} + \left\|\frac{f}{r}\right\|^2_{L^2(R^3)}. \tag{3.14c}$$

One can easily verify that the operator $\mathcal{L}$ can be represented as

$$\mathcal{L}(\cdot) = -r\Delta_5\left(\frac{\cdot}{r}\right), \tag{3.15}$$

where Δ_5 is the 5D Laplace operator

$$\Delta_5 = \partial_r^2 + \frac{3}{r}\partial_r + \partial_z^2.$$

With the above preparation (3.14), (3.15), we can now prove Lemma 3.4.

Proof Using (3.14) with $F^\theta = \frac{v^r v^\theta}{r}$, $\varphi = 0$, we have

$$\left\|D^4\frac{v^r v^\theta \mathbf{e}_\theta}{r}\right\|_{L^2(R^3)} = \left\|\mathcal{L}^2\frac{v^r v^\theta}{r}\right\|_{L^2(R^3)}.$$

Then using (3.15), we have

$$\left\|\mathcal{L}^2\frac{v^r v^\theta}{r}\right\|_{L^2(R^3)} = \left\|r\Delta_5^2\frac{v^r v^\theta}{r^2}\right\|_{L^2(R^3)} = \left\|\Delta_5^2\frac{v^r v^\theta}{r^2}\right\|_{L^2(R^5)} = \left\|D^4\frac{v^r v^\theta}{r^2}\right\|_{L^2(R^5)}.$$

Then using estimate (3.12), we have

$$\left\|D^4\frac{v^r v^\theta \mathbf{e}_\theta}{r^2}\right\|_{L^2(R^3)} \leq c\left\|\frac{v^r}{r}\right\|_{L^\infty}\left\|D^4\frac{v^\theta}{r}\right\|_{L^2(R^5)} + c\left\|\frac{v^\theta}{r}\right\|_{L^\infty}\left\|D^4\frac{v^r}{r}\right\|_{L^2(R^5)}. \tag{3.16}$$

Since v^r, v^θ vanish on the symmetric axis, we have

$$\left|\frac{v^r}{r}\right|, \quad \left|\frac{v^\theta}{r}\right| \leq \|\nabla\mathbf{v}\|_{L^\infty}. \tag{3.17}$$

Next, we estimate $\|D^4\frac{v^\theta}{r}\|_{L^2(R^5)}$ and $\|D^4\frac{v^r}{r}\|_{L^2(R^5)}$. We have that

$$\left\|D^4\frac{v^\theta}{r}\right\|_{L^2(R^5)} = \left\|\Delta_5^2\frac{v^\theta}{r}\right\|_{L^2(R^5)} = \left\|\frac{1}{r}\mathcal{L}^2 v^\theta\right\|_{L^2(R^5)} = \left\|\mathcal{L}^2 v^\theta\right\|_{L^2(R^3)}, \tag{3.18}$$

where we have used (3.15) in the second equality and change of measure in the third equality. Therefore, using (3.14) with $\mathbf{F} = \mathbf{v}$, we have

$$\left\| D^4 \frac{v^\theta}{r} \right\|_{L^2(R^5)} = \|\mathcal{L}^2 v^\theta\|_{L^2(R^3)} \leq \|\mathbf{v}\|_{H^4(R^3)}. \tag{3.19}$$

Similarly, using (3.15) and change of measure as in (3.18), we have

$$\left\| D^4 \frac{v^r}{r} \right\|_{L^2(R^5)} = \|\mathcal{L}^2 v^r\|_{L^2(R^3)} = \|\partial_z \mathcal{L}^2 \phi^\theta\|_{L^2(R^3)}. \tag{3.20}$$

Then according to (3.14) with $\mathbf{F} = \mathbf{v}$, we have

$$\left\| D^4 \frac{v^r}{r} \right\|_{L^2(R^5)} = \|\partial_z \mathcal{L}^2 \phi^\theta\|_{L^2(R^3)} \leq \|\mathbf{v}\|_{H^4(R^3)}. \tag{3.21}$$

Finally using (3.17), (3.19) and (3.21) in (3.16), we finish the proof. $\square$

Now we prove the BKM Theorem 3.3 for the inviscid model (2.15).

Proof Taking D^α with $|\alpha| = 4$ for both sides of Eq. (2.15), and computing its L^2 inner product with $D^\alpha v$, we get

$$\frac{1}{2}\frac{d}{dt}\|D^\alpha \mathbf{v}\|_{L^2(R^3)}^2 = -\epsilon(D^\alpha \mathbf{v}, D^\alpha(\mathbf{v} \cdot \nabla \mathbf{v})) + \left(D^\alpha \mathbf{v}, D^\alpha \frac{v^r v^\theta \mathbf{e}^\theta}{r} \right), \quad (3.22)$$

where we have used $(\cdot, \cdot)$ to denote the L^2 inner product on R^3.

Using the divergence-free condition, we have

$$(D^\alpha \mathbf{v}, \mathbf{v} \cdot D^\alpha \mathbf{v}) = 0.$$

Then for the first term on the right-hand side of (3.22), we have

$$-(D^\alpha \mathbf{v}, D^\alpha(\mathbf{v} \cdot \nabla \mathbf{v})) = -(D^\alpha \mathbf{v}, D^\alpha(\mathbf{v} \cdot \nabla \mathbf{v}) - \mathbf{v} \cdot D^\alpha \mathbf{v}).$$

Using the Hölder inequality and estimate (3.13), we have

$$-(D^\alpha \mathbf{v}, D^\alpha(\mathbf{v} \cdot \nabla \mathbf{v})) \leq C\|D^\alpha \mathbf{v}\|_{L^2(R^3)}\|\nabla \mathbf{v}\|_{L^\infty}\|D^\alpha \mathbf{v}\|_{L^2(R^3)}.$$

For the second term on the right-hand side of (3.22), using Lemma (3.4), we have

$$\left(D^\alpha \mathbf{v}, D^\alpha \frac{v^r v^\theta \mathbf{e}_\theta}{r} \right) \leq C\|\nabla \mathbf{v}\|_{L^\infty}\|D^\alpha \mathbf{v}\|_{L^2(R^3)}^2.$$

Putting these estimates in (3.22), we have

$$\frac{d}{dt}\|D^\alpha \mathbf{v}\|_{L^2(R^3)}^2 \leq C\|\nabla \mathbf{v}\|_{L^\infty}\|\mathbf{v}\|_{H^4}^2. \tag{3.23}$$

This together with the L^2 estimate (3.4), and the estimate (3.11), gives

$$
\begin{aligned}
&\|\mathbf{v}(t)\|_{H^4}^2 - \|\mathbf{v}(0)\|_{H^4}^2 \\
&\quad \leq C \int_0^t \|\mathbf{v}(s)\|_{H^4} (1 + \|\nabla \times \mathbf{v}\|_{\mathrm{BMO}} \ln(1 + \|\mathbf{v}(s)\|_{H^4}^2)) \mathrm{d}s.
\end{aligned}
$$

Then using the Gronwall's inequality and (3.10), we finish the proof that

$$
\|\mathbf{v}(T)\|_{H^4(R^3)} < +\infty.
$$

$\square$

For the viscous model (2.15) with $\nu > 0$, we have the following Prodi–Serrin type non-blow-up criterion.

Theorem 3.5 *For smooth solutions to (2.15) with $\mathbf{v}(x, 0) \in H^1(R^3)$, if*

$$
\mathbf{v}(x, t) \in L^q(L^p(R^3), [0, T)), \tag{3.24}
$$

with

$$
\frac{3}{p} + \frac{2}{q} = 1, \quad 3 < p \leq +\infty,
$$

then the solutions can be smoothly extended beyond T.

We need the following 1D Hardy inequality to estimate the additional stirring term in (2.15); see Hardy et al. (1952).

Lemma 3.6 *If $\lambda > 1$, $\sigma > 1$, $f(r)$ is a nonnegative measurable function, and $F(r)$ is defined by*

$$
F(r) = \int_0^r f(t) \mathrm{d}t,
$$

then

$$
\int_0^\infty r^{-\sigma} F^\lambda \mathrm{d}r \leq \left(\frac{\lambda}{\sigma - 1} \right)^\lambda \int_0^\infty r^{-\sigma} (rf)^\lambda \mathrm{d}r. \tag{3.25}
$$

Now we prove Theorem 3.5 using Lemma (3.6). We only consider the case that $3 < p < +\infty$, and the case that $p = +\infty$ is easier.

Proof Multiplying both sides of Eq. (2.15) by $-\Delta \mathbf{v}$, we get

$$
\frac{1}{2} \frac{d}{dt} \|\nabla \mathbf{v}\|_{L^2}^2 \leq \int_{R^3} |\Delta \mathbf{v}| |\mathbf{v}| |\nabla \mathbf{v}| \mathrm{d}x + \int_{R^3} |\Delta \mathbf{v}| \left| \frac{v^r v^\theta}{r} \right| \mathrm{d}x - \nu \|\Delta \mathbf{v}\|_{L^2}^2. \tag{3.26}
$$

Using the Hölder inequality, we have the following estimate for the first term on the right-hand side of (3.26),

$$
\begin{aligned}
\int_{R^3} |\Delta \mathbf{v}| |\mathbf{v}| |\nabla \mathbf{v}| \mathrm{d}x &\le \frac{\nu}{4} \|\Delta \mathbf{v}\|_{L^2}^2 + C \int_{R^3} |\mathbf{v}|^2 |\nabla \mathbf{v}|^2 \mathrm{d}x \\
&\le \frac{\nu}{4} \|\Delta \mathbf{v}\|_{L^2}^2 + C \|\mathbf{v}\|_{L^p}^2 \|\nabla \mathbf{v}\|_{L^{2p/(p-2)}}^2.
\end{aligned}
\tag{3.27}
$$

For the second term on the right-hand side of (3.26), using Hölder inequality twice, we have

$$
\begin{aligned}
\int_{R^3} |\Delta \mathbf{v}| |v^\theta| \left| \frac{v^r}{r} \right| \mathrm{d}x &\le \frac{\nu}{4} \|\Delta \mathbf{v}\|_{L^2}^2 + C \int_{R^3} |v^\theta|^2 \left| \frac{v^r}{r} \right|^2 \mathrm{d}x \\
&\le \frac{\nu}{4} \|\Delta \mathbf{v}\|_{L^2}^2 + C \|\mathbf{v}\|_{L^p}^2 \left(\int_{R^3} \frac{(v^r)^{2p/(p-2)}}{r^{2p/(p-2)}} \mathrm{d}x \right)^{\frac{p}{p-2}}.
\end{aligned}
\tag{3.28}
$$

Changing the integral to the cylindrical coordinates, we have

$$
\int_{R^3} \frac{(v^r)^{2p/(p-2)}}{r^{2p/(p-2)}} \mathrm{d}x = \int_R \int_0^\infty \frac{(v^r)^{2p/(p-2)}}{r^{(p+2)/(p-2)}} \mathrm{d}r \mathrm{d}z.
\tag{3.29}
$$

Since $v^r = 0$ on the symmetric axis, using estimate (3.25) with $F(r) = v^r$, $f(r) = \partial_r v^r$, $\sigma = \frac{p+2}{p-2}$, $\lambda = \frac{2n}{n-2}$, we get

$$
\begin{aligned}
\int_R \int_0^\infty \frac{(v^r)^{2p/(p-2)}}{r^{(p+2)/(p-2)}} \mathrm{d}r \mathrm{d}z &\le C \int_R \int_0^\infty r (v_r^r)^{2p/(p-2)} \mathrm{d}r \mathrm{d}z \\
&\le C \int_{R^3} |\nabla \mathbf{v}|^{2p/(p-2)} \mathrm{d}x.
\end{aligned}
\tag{3.30}
$$

Substituting (3.30) and (3.29) in (3.28), we get

$$
\int |\Delta \mathbf{v}| |v^\theta| \left| \frac{v^r}{r} \right| \mathrm{d}x \le \frac{\nu}{4} \|\Delta \mathbf{v}\|_{L^2}^2 + C \|\mathbf{v}\|_{L^p}^2 \|\nabla \mathbf{v}\|_{L^{2p/(p-2)}}^2.
\tag{3.31}
$$

Finally we use the Gagliardo–Nirenberg interpolation inequality (Nirenberg 1959),

$$
\|\nabla \mathbf{v}\|_{L^{2p/(p-2)}}^2 \le C \|\nabla \mathbf{v}\|_{L^2}^{4/q} \|\Delta \mathbf{v}\|_{L^2}^{6/p}.
\tag{3.32}
$$

Putting the estimates (3.27), (3.31), (3.32) in (3.26), we have

$$
\frac{d}{dt} \|\nabla \mathbf{v}\|_{L^2}^2 \le C \|\mathbf{v}\|_{L^p}^2 \|\nabla \mathbf{v}\|_{L^2}^{\frac{4}{q}} \|\Delta \mathbf{v}\|_{L^2}^{6/p} - \frac{\nu}{2} \|\Delta \mathbf{v}\|_{L^2}^2.
$$

Then using the Hölder inequality and the fact that $\frac{2}{q} + \frac{3}{p} = 1$, we get

$$\frac{d}{dt}\|\nabla\mathbf{v}\|_{L^2}^2 \leq C\|\mathbf{v}\|_{L^p}^q\|\nabla\mathbf{v}\|_{L^2}^2. \tag{3.33}$$

Using (3.24) in (3.33), we can finish the proof of the theorem. $\square$

4 Self-Similar Singularity of the Inviscid Models with Weak Convection

In this section, we numerically study the inviscid models (2.8) with different values of ϵ. We employ two approaches in our numerical investigation, the direct numerical simulation and the dynamic rescaling formulation. In the direct numerical simulation, we observe that with weak convection the numerical solutions develop self-similar singularity with the singular region traveling along the symmetric axis, and such singularity formation scenario does not persist for strong convection. Then we introduce the dynamic rescaling formulation that governs the evolution of the spatial profiles in the singular solutions and demonstrate the linear stability of the traveling self-similar singularity.

4.1 Direct Numerical Simulation of the Models

We consider solving the inviscid models (2.8) in a periodic cylinder,

$$(r, z) \in [0, 1] \times [0, 2],$$

with no-flow boundary condition. The no-flow boundary condition requires the following boundary condition for the Poisson equation (2.4c),

$$\phi_1|_{r=1} = 0.$$

For $\epsilon = 0$, we choose the following initial data

$$\omega_1(r, z) = 0, \quad u_1(r, z) = 300 \sin^{20}\left(\frac{\pi}{2}z\right)(r^2 - 1)^{40}. \tag{4.1}$$

Then according to Eq. (2.4), ω_1 will remain odd at $z = 0$ and $z = 1$, and u_1 will remain even at $z = 0$ and $z = 1$. Thus in our numerical simulation, we only need to solve the equations on a computational domain

$$D = (r, z) \in [0, 1] \times [0, 1]. \tag{4.2}$$

The stream function ϕ_1 will also remain odd at $z = 0$ and $z = 1$, so in solving the Poisson equation (2.4c), we can use the following boundary condition

$$\phi_1|_{\partial D} = 0.$$

Our preliminary numerical results suggest that the models with weak convection develop finite-time singularity on the symmetric axis. To resolve the singularity, one needs a very fine mesh in the singular region, and in our numerical simulation, we employ an adaptive mesh method introduced by Luo and Hou (2014). We consider a change of variables that maps $(\rho, \eta) \in [0, 1]^2$ to $(r, z) \in [0, 1]^2$, with the derivatives $r_\rho(\rho)$ and $z_\eta(\eta)$ parameterized as

$$r_\rho = \alpha_1 + \alpha_2 e^{-\pi(\rho-1)^2/\sigma_1^2}, \tag{4.3a}$$

$$z_\eta = \alpha_3 + \alpha_4 e^{-\pi\eta^2/\sigma_2^2} + \alpha_5 e^{-\pi(\eta-1)^2/\sigma_3^2}. \tag{4.3b}$$

We use a uniform mesh in the (ρ, η) space in our simulation and choose the parameters α_i and σ_j in (4.3) such that a certain portion of the node points is put in the "singular region." In the r direction we would like to put δ portion of the node points in the "singular region" $[0, r_0]$. We first choose

$$\sigma_1 = (1 - \delta) \times \frac{2}{5}, \tag{4.4}$$

such that the exponential part in r_ρ is negligible for $\rho \in [0, \delta]$,

$$e^{-\pi(\rho-1)^2/\sigma_1^2} \le e^{-\frac{25\pi}{4}} \approx 0, \tag{4.5}$$

which means we use a nearly uniform mesh in the "singular region" $[0, r_0]$.

Then we choose α_1 and α_2 such that

$$r(\rho)|_{\rho=\delta} = r_0, \quad r(\rho)|_{\rho=1} = 1,$$

which according to (4.5) leads to the following linear system

$$\alpha_1\delta = r_0, \quad \alpha_1 + \frac{1}{2}\sigma_1\alpha_2 = 1 \Rightarrow \alpha_1 = r_0/\delta, \quad \alpha_2 = \frac{5(\delta - r_0)}{\delta(1 - \delta)}. \tag{4.6}$$

Thus for $r_0 \le \delta$, we can uniquely determine $\alpha_1 > 0, \alpha_2 > 0$ and $\sigma_1 > 0$ in (4.3).

In the z direction, we would like to put δ portion of the node points in the "singular region" $[z_1, z_2]$. We first determine the portion of node points put in the left and right intervals $[0, z_1]$ and $[z_2, 1]$, denoted by δ_1 and δ_2, as

$$\delta_1 = \frac{z_1}{z_1 + 1 - z_2}(1 - \delta), \quad \delta_2 = \frac{1 - z_2}{z_1 + 1 - z_2}(1 - \delta), \tag{4.7}$$

which guarantees that the portions of node points in the "regular regions," $[0, z_1]$ and $[z_2, 1]$, are proportional to the length of the intervals.

Next we choose σ_2 and σ_3 based on δ_1 and δ_2 (4.7) as

$$\sigma_2 = \delta_1 \times \frac{2}{5}, \quad \sigma_3 = \delta_2 \times \frac{2}{5}, \tag{4.8}$$

such that the exponential part in z_η is negligible for $\eta \in [\delta_1, 1 - \delta_2]$,

$$e^{-\pi\eta^2/\sigma_2^2}, \ e^{-\pi(\eta-1)^2/\sigma_3^2} \approx 0. \tag{4.9}$$

Finally we choose α_3, α_4 and α_5 such that

$$z(\eta)|_{\eta=\delta_1} = z_1, \quad z(\eta)|_{\eta=1-\delta_2} = z_2, \quad z(\eta)|_{\eta=1} = 1,$$

which according to (4.9) leads to the linear system

$$\begin{cases} \alpha_3\delta_1 + \frac{1}{2}\alpha_4\sigma_2 = z_1, \\ \alpha_3(\delta_1 + \delta) + \frac{1}{2}\alpha_4\sigma_2 = z_2, \quad \Rightarrow \\ \alpha_3 + \frac{1}{2}\alpha_4\sigma_2 + \frac{1}{2}\alpha_5\sigma_3 = 1, \end{cases} \begin{cases} \alpha_3 = \frac{z_2-z_1}{\delta}, \\ \alpha_4 = 5\frac{\delta(1-z_2+z_1)-(1-\delta)(z_2-z_1)}{(1-\delta)\delta}, \\ \alpha_5 = 5\frac{\delta(1-z_2+z_1)-(1-\delta)(z_2-z_1)}{(1-\delta)\delta}. \end{cases} \tag{4.10}$$

Then for $z_2 - z_1 \leq \delta$, we can determine $\sigma_2, \sigma_3 > 0$ and $\alpha_j > 0$ ($j = 3, 4, 5$) in (4.3).

The conditions (4.5), (4.9) guarantee that the transforms (4.3) are even at $r = 0$ and $z = 0, 1$. With the change of variables, Eqs. (2.4) become

$$u_{1,t} + u^r \frac{u_{1,\rho}}{r_\rho} + u^z \frac{u_{1,\eta}}{z_\eta} = 2u_1 \frac{\phi_{1,\eta}}{z_\eta}, \tag{4.11a}$$

$$\omega_{1,t} + u^r \frac{\omega_{1,\rho}}{r_\rho} + u^z \frac{\omega_{1,\eta}}{z_\eta} = 2u_1^2 \frac{u_{1,\eta}}{z_\eta}, \tag{4.11b}$$

with the velocity field given by

$$u^r = -\epsilon r \frac{\phi_{1,\eta}}{z_\eta}, \quad u^z = 2\epsilon\phi_1 + \epsilon r \frac{\phi_{1,\eta}}{r_\eta}. \tag{4.11c}$$

The weak form of the Poisson equation (2.4c) becomes,

$$\begin{aligned} a(\phi_1, \psi) &= \int_{[0,1]^2} \left(\frac{\phi_{1,\rho}}{r_\rho} \frac{\psi_\rho}{r_\rho} + \frac{\phi_{1,\eta}}{z_\eta} \frac{\psi_\eta}{z_\eta} \right) r^3 r_\rho z_\eta \mathrm{d}\rho d\eta \\ &= \int_{[0,1]^2} \omega_1 \psi r^3 r_\rho z_\eta \mathrm{d}\rho d\eta, \quad \forall \psi \in V, \end{aligned} \tag{4.11d}$$

where

$$V = \mathrm{span}\{\psi \in H^1[0,1]^2 : \psi(-\rho, \eta) = \psi(\rho, \eta),$$
$$\psi(1, \eta) = \psi(r, 0) = \psi(r, 1) = 0\}.$$

We discretize the computational domain (ρ, η) using a uniform mesh

$$(\rho_i, \eta_j) = (ih_\rho, jh_\eta), \quad 0 \leq i \leq N_R, \quad 0 \leq j \leq N_Z,$$

where $h_\rho = \frac{1}{N_R}$ and $h_\eta = \frac{1}{N_Z}$ are the uniform mesh sizes.

We use a second-order center difference scheme to compute the derivatives $\phi_{1,z}$ and $\phi_{1,r}$ in (4.11c), the derivatives in the convection terms of (4.11a) and (4.11b), and the derivatives in the nonlinear vortex stretching terms.

We discretize the Poisson equation (4.11d) using a finite-element method with trial space

$$V_h = \{\psi(r, z) \in V : \psi(r, z) \text{ is piecewise bilinear}\}.$$

In the temporal direction, we use the fourth-order explicit Runge–Kutta method and choose the time step size Δt such that the CFL number

$$\frac{|u^r|\Delta t}{h_\rho}, \quad \frac{|u^z|\Delta t}{h_\eta} \leq 0.5, \tag{4.12a}$$

and the growth of maximum ω_1 in each time step does not exceed 1%, namely

$$\|w_1^{n+1}\|_{L^\infty} - \|w_1^n\|_{L^\infty} \leq (\|w_1^n\|_{L^\infty} + 10) \times 1\%. \tag{4.12b}$$

In our simulation, we identify the "singularity region" of the solutions as

$$(r, z) \in [0, L] \times \left[-\frac{L}{2} + c, \frac{L}{2} + c\right],$$

where $(r, z) = (0, c)$ is the position where maximum ω_1 is attained, $\omega_1(0, c) = \|\omega_1\|_{L^\infty}$, and L is chosen such that $\omega_1(L, c) = \frac{1}{2}\omega_1(0, c)$.

We use two sets of mesh in our simulation with

$$N_R = N_Z = 512, \quad \text{and} \quad N_R = N_Z = 1024. \tag{4.13}$$

We simulate the model (4.11) with $\epsilon = 0$ using initial data (4.1) until $\|\omega_1\|_{L^\infty}$ reaches 1.1×10^8. In the simulation, we keep track of $\|\omega_1(t)\|_{L^\infty}$, $\|u_1(t)\|_{L^\infty}$, which are attained on the symmetric axis, and record the numerical solutions at time steps corresponding to different $\|\omega_1(t)\|_{L^\infty}$. The growth of $\log \|u_1(t)\|_{L^\infty}$ and $\log \|\omega_1(t)\|$ is plotted in Fig. 1, and we can see that there exists very small difference between the results obtained on the two meshes (4.13). In the rest of this paper, we will only present numerical results on the fine mesh.

Then we use the numerical solutions for $\epsilon = 0$ at the time step $\|\omega_1\|_{L^\infty} = 3 \times 10^4$ as initial data for the model with different ϵ,

$$\epsilon = 0.1, \quad \epsilon = 0.2, \quad \epsilon = 0.3, \quad \epsilon = 0.4.$$

The decay of the inverse of $\|u_1(t)\|_{L^\infty}$ is plotted in Fig. 2. We can see that for weak convection, $\|u_1(t)\|_{L^\infty}$ goes to infinity and the models develop finite-time singularity, while for strong convection, such finite-time singularity scenario does not
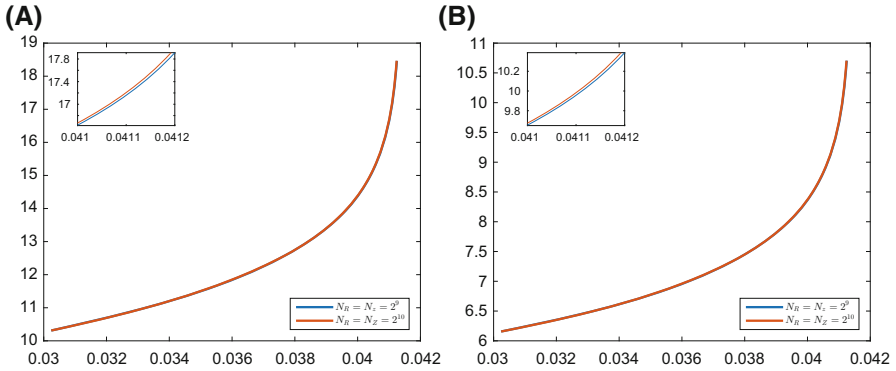
Fig. 1 Resolution study using two meshes. **a** $\log \|\omega_1(t)\|_{L^\infty}$. **b** $\log \|u_1(t)\|_{L^\infty}$
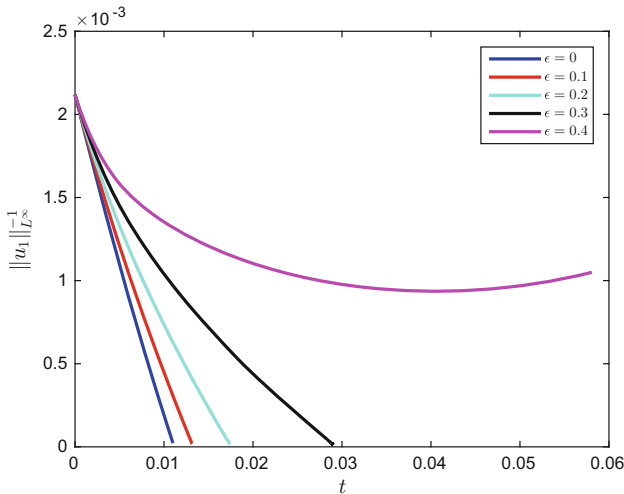

Fig. 2 Finite-time singularity for weak convection

persist. Moreover, we can see that close to the singularity time, $\|u_1(t)\|_{L^\infty}^{-1}$ decays approximately linearly for weak convection,

$$\|u_1(t)\|_{L^\infty}^{-1} \approx C(T - t).$$

For the case $\epsilon = 0.2$, the numerical solutions restricted on the symmetric axis at several different time steps are plotted in Fig. 3, and we can see that the center of the singularity region is not stationary but traveling along the symmetric axis. The singularity scenario for $\epsilon = 0, 0.1, 0.3$ is similar.

Next we consider the spatial profiles in the solutions as approaching the potential singularity time. In this paper we refer to "profile" as normalized solutions. At time t, the spatial profiles $U(t)$ and $W(t)$ are obtained as
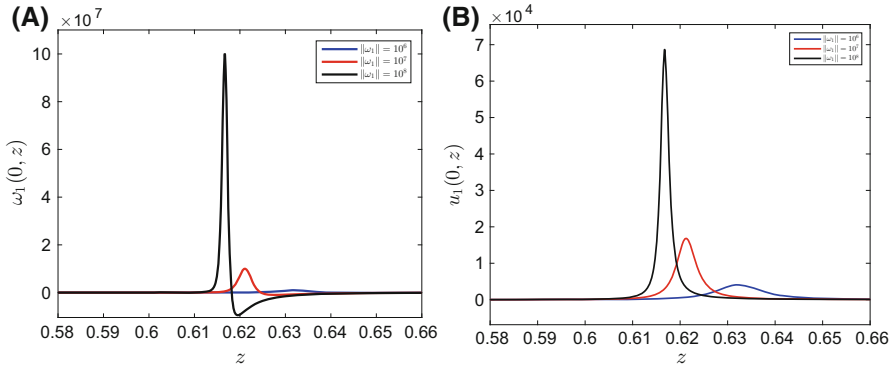
Fig. 3 The traveling of the singularity region. **a** $\omega_1(0, z, t)$. **b** $u_1(0, z, t)$

$$U(t) = \frac{1}{\tau} u_1\left(\frac{r}{\lambda}, \frac{z-c}{\lambda}, t\right), \quad W(t) = \frac{1}{\lambda\tau}\omega_1\left(\frac{r}{\lambda}, \frac{z-c}{\lambda}, t\right), \quad (4.14a)$$

where the scaling and shifting are based on the scaling and translational invariance property of the model (3.1), (3.3). We choose the parameter c in (4.14) such that the singularity region is shifted to the origin. The solution $\omega(0, z, t)$ crosses zero once in the singularity region, and we choose c such that

$$W(0, 0, t) = 0. \quad (4.14b)$$

And we choose λ and τ to normalize $W_z(0, 0, t)$ and $U(0, 0, t)$,

$$W_z(0, 0, t) = C_1, \quad U(0, 0, t) = C_2. \quad (4.14c)$$

For $\epsilon = 0.2$, we consider the spatial profiles in the singular solutions at different time steps corresponding to different $\|\omega_1\|_{L^\infty}$. To simplify our presentation, we only plot the profiles restricted on the symmetric axis in Fig. 4. We can see that the profiles at different time steps close to the singularity time collapse, which implies the self-similar nature of the finite-time singularity. In this paper, by self-similar singularity we mean that the spatial profiles in the singular solutions converge as approaching the singularity time. For the cases $\epsilon = 0, 0.1, 0.3$, the singular solutions also exhibit self-similar feature.

Based on the singularity scenario described above, we make the following self-similar ansatz for the singular solutions close to the singularity time:

$$u_1 = (T-t)^{c_u} U\left(\frac{r}{(T-t)^{c_l}}, \frac{z-c(t)}{(T-t)^{c_l}}\right), \quad (4.15a)$$

$$\omega_1 = (T-t)^{c_\omega} W\left(\frac{r}{(T-t)^{c_l}}, \frac{z-c(t)}{(T-t)^{c_l}}\right). \quad (4.15b)$$
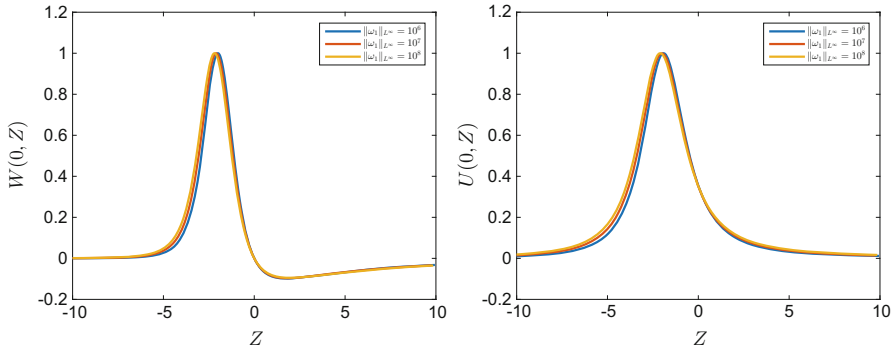
Fig. 4 Profiles of the singular solutions on the symmetric axis

In the above ansatz, $(r, z) = (0, c(t))$ is the center of the singularity region, and $U(r, z)$, $W(r, z)$ are the self-similar profiles of the singular solutions. The exponents c_u, c_ω and c_l characterize the blow-up rate of the solutions.

Plugging the above self-similar ansatz into Eq. (2.5), and matching the order of $(T - t)$ for each term in the equations, we get

$$c_u = -1, \quad c_\omega = -1 - c_l, \quad \frac{d}{dt}c(t) = c(T - t)^{c_l - 1}, \tag{4.16a}$$

and the following self-similar equations governing the self-similar profiles,

$$U + (c_l r + U^r)U_r + (c_l z + U^z - c)U_z = 2U\Psi_z, \tag{4.16b}$$

$$(c_l + 1)W + (c_l r + U^r)W_r + (c_l z + U^z - c)W_z = (U^2)_z, \tag{4.16c}$$

$$-\left[\partial_r^2 + (3/r)\partial_r + \partial_z^2\right]\Psi = W, \tag{4.16d}$$

where

$$U^r = -\epsilon r\Phi_z, \quad U^z = 2\epsilon\Phi + \epsilon r\Phi_r. \tag{4.16e}$$

To study the self-similar Eq. (4.16), we can make the following scaling transformation,

$$U_c(r, z) \rightarrow U\left(\frac{r}{c}, \frac{z}{c}\right), \quad W_c(r, z) \rightarrow \frac{1}{c}W\left(\frac{r}{c}, \frac{z}{c}\right),$$

and the scaled profiles W_c and U_c will satisfy the same self-similar equations with c changed to $c = 1$. In another word, the unknown parameter c can be chosen to be 1 based on scaling of the profiles.

However, the exponent c_l in (4.16) cannot be determined by a simple scaling argument and it is the only unknown scaling parameter. In the literature (Barenblatt and Zel'Dovich 1972; Sedov 1993), such singularity is called self-similar singularity of
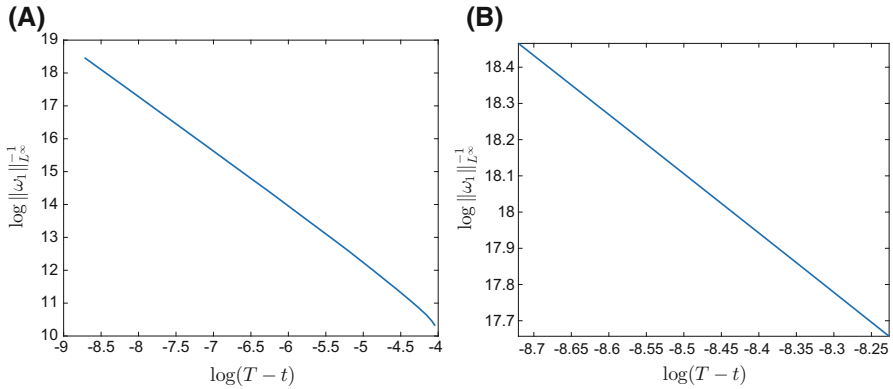
(A)

(B)

Fig. 5 Linear regression to determine c_ω. **a** $\log \|\omega_1(t)\|_{L^\infty}$. **b** Linear regression region

Table 1 The scaling exponent c_l for different ϵ

ϵ	0.0	0.1	0.2	0.3
c_l	0.744	0.689	0.636	0.578

the second kind, and to solve Eq. (4.16), one needs to find c_l such that the equations have non-trivial solutions, which is essentially a nonlinear eigenvalue problem.

In Fig. 2, we can see that for weak convection, the inverse of $\|u_1(t)\|_{L^\infty}$ decays linearly close to the singularity time, which agrees with the scaling exponent $c_u = -1$ obtained in (4.16a). Using this we compute the approximate singularity time T by linear regression on a time interval close to singularity,

$$\|u_t(t)\|_{L^\infty}^{-1} \approx C_1 t + C_2, \quad T \approx -\frac{C_2}{C_1}. \tag{4.17}$$

Next we use the estimated singularity T from (4.17) in linear regression

$$\log \|\omega_1(t)\|_{L^\infty} \approx c_\omega \log(T - t) + C, \tag{4.18}$$

on the same time interval as (4.17) to determine the scaling exponent c_ω. And after we get c_ω, the exponent c_l can be obtained as

$$c_l = -c_\omega - 1.$$

The region of linear regression (4.18) in the case that $\epsilon = 0.2$ is plotted in Fig. 5. The estimated c_l for $\epsilon = 0, 0.1, 0.2, 0.3$ are listed in Table 1. We can see that as the strength of the convection increases, the scaling exponent c_l becomes smaller; namely, the length scale of the solutions decays slower.

Due to the nonlinear and nonlocal nature of the self-similar Eq. (4.16), it is difficult to prove the existence of c_l such that (4.16) has non-trivial solutions, which is essentially a nonlinear eigenvalue problem. In the next subsection, we employ a dynamic

rescaling formulation, which governs the evolution of the spatial profiles (4.14) in the singular solutions, to numerically demonstrate the stability of the observed self-similar singularity.

4.2 Stability of the Self-Similar Singularity

According to the self-similar Eq. (4.16), if the solutions to (2.8) start from initial data equal to the self-similar profiles, then the profiles in the singular solutions will remain the same, and the solutions will develop singularity exactly as the ansatz (4.15). In this subsection, we consider the stability of the self-similar profiles and demonstrate that the solutions to (2.8) develop singularity asymptotically as (4.15) if starting from initial data that are perturbed from the self-similar profiles.

We demonstrate the stability of the self-similar profiles using the dynamic rescaling formulation. We add scaling terms to Eq. (2.4) and get

$$u_{1,t} + (c_l(t)r + u^r)u_{1,r} + (c_l(t)z + u^z + c(t))u_{1,z} = 2u_1\phi_{1,z} + c_u(t)u_1, \quad (4.19a)$$

$$\omega_{1,t} + (c_l(t)r + u^r)\omega_{1,r} + (c_l(t)z + u^z + c(t))\omega_{1,z} = (u_1^2)_z + c_\omega(t)\omega_1, \quad (4.19b)$$

$$-\left[\partial_r^2 + (3/r)\partial_r + \partial_z^2\right]\phi_1 = \omega_1, \quad (4.19c)$$

where the velocity field above is the same as the original equations,

$$u^r = -\epsilon r\phi_{1,z}, \quad u^z = 2\epsilon\phi_1 + \epsilon r\phi_{1,r}.$$

In the above formulation, the $c_l(t)r\partial_r$, $c_l(t)z\partial_z$ terms stretch the solutions in the spatial direction; the $c(t)\partial_z$ term shifts the solutions along the axial direction; the $c_\omega(t)\omega_1$ and $c_u(t)u$ terms rescale the solutions ω_1 and u_1 in amplitude, respectively. According to the scaling invariance property of the model (3.1), we need to choose the following condition for the scaling parameters in (4.19),

$$c_\omega(t) = c_u(t) - c_l(t) \quad (4.19d)$$

such that the dynamic rescaling equations are equivalent to the 3D models.

To be specific, let $u_1(r, z, t)$, $\omega_1(r, z, t)$ be solutions to the model (2.5), then

$$u_1(r, z, t) = C_u(t)u_1\left(C_l(t)r, C_l(t)z - z(t), \tau(t)\right), \quad (4.20a)$$

$$\omega_1(r, z, t) = C_\omega(t)\omega_1\left(C_l(t)r, C_l(t)z - z(t), \tau(t)\right), \quad (4.20b)$$

are solutions to the dynamic rescaling Eq. (4.19), where

$$\frac{d}{dt}\tau(t) = \exp\left(\int_0^t c_u(s)ds\right), \quad (4.20c)$$

$$C_u(t) = \exp\left(\int_0^t c_u(s)ds\right), \quad (4.20d)$$

$$C_\omega(t) = \exp\left(\int_0^t c_\omega(s)\mathrm{d}s\right), \tag{4.20e}$$

$$C_l(t) = \exp\left(\int_0^t -c_l(s)\mathrm{d}s\right), \tag{4.20f}$$

$$z(t) = \int_0^t c(s)C_l(s)\mathrm{d}s. \tag{4.20g}$$

In another word, the solutions to the dynamic rescaling Eq. (4.19) are simply rescaling of the solutions to the original Eq. (2.4).

To fix the scaling parameters in the above dynamic rescaling formulation, we need suitable normalization conditions. We first fix the center of the solution at the origin. In another word, we choose $c(t)$ in (4.19) such that

$$\omega_1(0, 0, t) = 0. \tag{4.21a}$$

The above condition leads to

$$c(t) = \frac{2u_1 u_{1,z}(0,0)}{\omega_{1,z}(0,0)} - u^z(0,0). \tag{4.21b}$$

Then we choose $c_l(t)$ and $c_u(t)$ to normalize the derivatives of w and the value of u at the origin. Namely, we choose $c_l(t)$ and $c_u(t)$ such that

$$\frac{d}{dt}\omega_{1,z}(0,0) = 0, \quad \frac{d}{dt}u(0,0) = 0. \tag{4.21c}$$

And this leads to the following $c_l(t)$ and $c_u(t)$,

$$c_u(t) = \frac{2(u_{1,z})^2}{\omega_{1,z}} - 2\phi_{1,z}, \tag{4.21d}$$

$$c_l(t) = \frac{(u_{1,z})^2}{\omega_{1,z}} - \phi_{1,z} - \frac{u_1 u_{1,z}\omega_{1,zz}}{\omega_{1,z}^2} - u_z^z + \frac{u_1 u_{1,zz} + (u_{1,z})^2}{\omega_{1,z}}. \tag{4.21e}$$

With the normalization conditions (4.21) and the equivalent relation (4.20), we conclude that the dynamic rescaling equations govern the evolution of the spatial profiles in the solutions (4.14). The self-similar profiles correspond to a steady state of the dynamic rescaling equations, and we will numerically study the stability of the steady state of (4.19) to demonstrate the stability of the singularity scenario described in the previous subsection.

A similar dynamic rescaling formulation has been employed to study the singularity of nonlinear Schrödinger equations in McLaughlin et al. (1986), Landman et al. (1988), LeMesurier et al. (1988), Landman et al. (1992) and Papanicolaou et al. (1994). In those works, the dynamic rescaling formulation is primarily used as an approach to accurately solve the equations numerically. In this work, we employ this formulation to investigate the stability of the self-similar profiles. In the works we just mentioned

above, the singular region is not traveling, so there is no need to add the shifting term $c(t)\partial_z$ as in (4.19). The normalization condition (4.21) is also different from those in the study of Schrödinger equations.

The dynamic rescaling Eqs. (4.19) are defined on unbounded domain

$$(r, z) \in R^+ \times R,$$

and to numerically solve the equations, we need to first truncate the equations to a bounded computational domain

$$(r, z) \in D = [0, M] \times [-M, M], \quad M = 120, \tag{4.22}$$

and discretize D using a uniform mesh

$$(r_i, z_j) = \left(ir_h, \left(j - \frac{nz}{2}\right)z_h\right), \quad 0 \le i \le nr, \quad 0 \le j \le nz, \tag{4.23}$$

where $r_h = M \times \frac{1}{nr}, z_h = M \times \frac{2}{nz}$.

To truncate the solutions ω_1 and u_1 to the computational domain D, we introduce the following projection operators,

$$P_u f(r, z) = P^r P_u^z f(r, z), \tag{4.24a}$$

$$P_\omega f(x) = P^r P_\omega^z f(r, z), \tag{4.24b}$$

where P^r, P_u^z and P_ω^z are defined as

$$P^r f(r, z) = f(r, z) - \frac{r^2}{M^2} f(M, z), \tag{4.24c}$$

$$P_u^z f(r, z) = f(r, z) - f(r, M)\frac{z(z + M)}{2M^2} - f(r, -M)\frac{z(z - M)}{2M^2}, \tag{4.24d}$$

$$P_\omega^z f(r, z) = f(r, z) - f(r, M)\frac{z^2(z + M)}{2M^3} + f(r, -M)\frac{z^2(z - M)}{2M^3}. \tag{4.24e}$$

Putting the above truncation operator in Eq. (4.19), we get

$$u_{1,t} = P_u(-(c_l(t)r + u^r)u_{1,r} - (c_l(t)z + u^z + c(t))u_{1,z} + 2u_1\phi_{1,z} + c_u(t)u_1),$$

$$\omega_{1,t} = P_\omega(-(c_l(t)r + u^r)\omega_{1,r} - (c_l(t)z + u^z + c(t))\omega_{1,z} + (u_1^2)_z + c_\omega(t)\omega_1).$$

The projection operators (4.24) do not change the evenness of ω_1 and u_1 with respect to r or violate the normalization condition (4.21). Moreover, if u_1 and ω_1 decay fast and are small on the boundary of the computational domain, then the error introduced by the projection operators is also small.

To compute the velocity field u^r and u^z, one needs to solve the Poisson equation (2.4c) on the computational domain D (4.22). To get the appropriate boundary

condition for ϕ_1, we write it using the 5D Green's function as

$$\phi_1(y) = \frac{1}{8\pi^2} \int_{R^5} \omega_1(y') \frac{1}{|y - y'|^3} dx'. \tag{4.25}$$

Since ϕ_1 and ω_1 are symmetric with respect to $y_{1,2,3,4}$, it is convenient to transform the integral (4.25) using the 4D spherical coordinates, and we get

$$\phi_1(r, z) = \frac{1}{8\pi^2} \int_R dz' \int_0^\infty dr' \int_0^\pi d\theta_1 \int_0^\pi d\theta_2 \int_0^{2\pi} d\theta_3 \tag{4.26}$$
$$r'^3 \sin^2 \theta_1 \sin \theta_2 ((r - r' \cos \theta_1)^2 + r'^2 \sin^2 \theta_1 + (z - z')^2)^{-3/2} \omega_1(r', z').$$

And it can be simplified as

$$\phi_1(r, z) = \frac{1}{8\pi^2} \int_R dz' \int_0^\infty dr' \omega_1(r', z') G(r, r', z), \tag{4.27}$$

where

$$G(r, r', z) = \frac{-4\pi r' \left((z - z')^2 + (r + r')^2\right) \text{EllipticE}\left(\frac{4rr'}{(z-z')^2+(r+r')^2}\right)}{r^2 \sqrt{(z - z')^2 + (r + r')^2}}$$
$$+ \frac{4\pi r' \left((z - z')^2 + r^2 + r'^2\right) \text{EllipticK}\left(\frac{4rr'}{(z-z')^2+(r+r')^2}\right)}{r^2 \sqrt{(z - z')^2 + (r + r')^2}}. \tag{4.28}$$

Here the function EllipticE is the complete elliptic integral of the second kind, and EllipticK is the complete elliptic integral of the first kind.

So to compute the velocity field, we first recover ω_1 as a piecewise bilinear function based on its values on the node points (4.23), and then we compute the value of ϕ_1 on the boundary of the computational domain using the integral formula (4.27). In evaluating the integral (4.27), we use the fourth-order Gaussian quadrature rule on each local piece of the domain. Then with the boundary condition, we solve the Poisson equation (4.19c) using a second-order finite element method and get the velocity field based on (2.8).

We use the upwind scheme to discretize the spatial derivatives in the convection terms in (4.19) and use the second-order center difference scheme to discretize the spatial derivatives in the vortex stretching terms. After the spatial discretization, we get an ODE system of $\vec{\omega}$ and $\vec{u}$,

$$\frac{d}{dt}\vec{u} = F_u(\vec{u}, \vec{\omega}), \quad \frac{d}{dt}\vec{\omega} = F_\omega(\vec{u}, \vec{\omega}). \tag{4.29}$$

Note that the determination of the scaling parameters (4.21), the numerical computation of the Biot–Savart law (4.27) and the truncation operators (4.24) are all encoded in the forcing functions F_u and F_ω in (4.29).

Table 2 The scaling exponent c_l obtained from dynamic rescaling

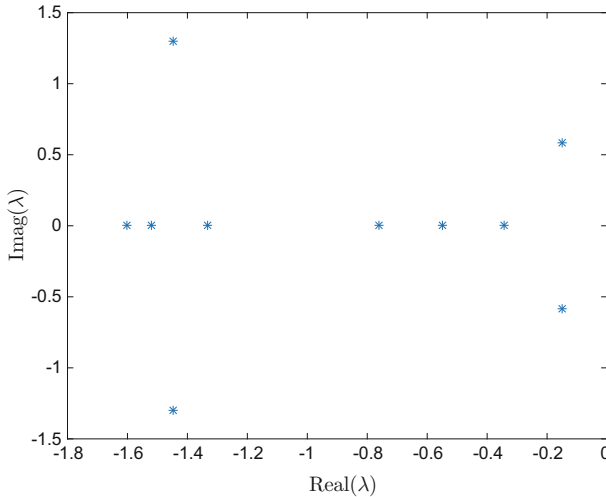| ϵ	0.0	0.1	0.15	0.18	0.19	0.2
c_l	0.962	0.864	0.823	0.798	0.792	0.784

Fig. 6 Distribution of the first several eigenvalues

We use the forward Euler scheme to numerically solve the ODE (4.29), and the time step size dt is chosen such that the CFL number is less than 0.5.

We use the rescaling of numerical solutions from direct numerical simulation of the models close to the singularity time as initial data for the dynamic rescaling Eq. (4.19). We observe that for small ϵ, the solutions converge to a steady state, which according to the equivalent relation between the solutions of the dynamic rescaling equations and the original model, (4.20), implies the asymptotic self-similar singularity of the models.

The scaling exponents c_l corresponding to different ϵ are listed in Table 2. We can see that c_l decays as we increase ϵ, which agrees with what we have observed in the direct numerical simulation of the models in Table 1.

However, there is some discrepancy between the scaling exponent c_l obtained from direct simulation of the models and the dynamic rescaling formulation. This is because of the error introduced by the truncation operators (4.24).

Next we numerically study the stability of the self-similar profiles. Recall that the self-similar profiles are the steady-state solutions of the dynamic rescaling equations, and the stability of the self-similar singularity is the stability of the steady state of the dynamic rescaling Eq. (4.19).

We numerically study the linear stability of the steady state of the ODE and compute the Jacobian matrix of its right-hand side

$$ J = \begin{bmatrix} \nabla_{\bar{u}} F_u & \nabla_{\bar{\omega}} F_u \\ \nabla_{\bar{u}} F_\omega & \nabla_{\bar{\omega}} F_\omega \end{bmatrix}. \tag{4.30} $$

Table 3 Largest real part of the eigenvalues

ϵ	0.0	0.1	0.15	0.18	0.19	0.2
max Real(λ_i)	−0.3449	−0.3345	−0.3634	−0.2851	−0.1815	−0.1499

The first few dominating eigenvalues with the largest real parts of the Jacobian matrix for $\epsilon = 0.2$ are plotted in Fig. 6. We can see that the eigenvalues have negative real part, which demonstrates the stability of the steady state and therefore the stability of the traveling wave self-similar singularity.

For different ϵ, the largest real parts of the eigenvalues of the Jacobian matrix (4.30) are listed in Table 3. From the table, we can see that for larger ϵ, the largest eigenvalue of the Jacobian matrix becomes larger, which means the self-similar singularity becomes less stable. This demonstrates the subtle balance between the convection and nonlinear vortex stretching terms and might explain the depletion of nonlinearity for strong convection.

5 Concluding Remarks

A family of 3D models for the axisymmetric incompressible Euler and Navier–Stokes equations are proposed. These models are derived by changing the strength of the convection terms of the axisymmetric Euler and Navier–Stokes equations written using a set of transformed variables. The family of models share several regularity results with the original Euler and Navier–Stokes equations, including an energy identity, the conservation of a modified circulation quantity and some non-blow-up criteria. Despite the similarities between the proposed models and the Euler equations, our numerical results suggest that the inviscid models with weak convection develop stable self-similar singularity with the singular region traveling along the symmetric axis, and such singularity scenario does not seem to persist for the original Euler equations. We use a dynamic rescaling formulation that governs the evolution of the spatial profiles in the singularity solutions to demonstrate the stability of the traveling self-similar singularity scenario. We observe that as the strength of the convection terms increases, the self-similar profiles become less stable, which shows the subtle balance between the nonlinear convection terms and the nonlinear vortex stretching terms.

References

Barenblatt, G.I., Zel'Dovich, Y.B.: Self-similar solutions as intermediate asymptotics. Ann. Rev. Fluid Mech. **4**(1), 285–312 (1972)

Beale, J.T., Kato, T., Majda, A.: Remarks on the breakdown of smooth solutions for the 3-D Euler equations. Commun. Math. Phys. **94**(1), 61–66 (1984)

Choi, K., Hou, T.Y., Kiselev, A., Luo, G., Sverak, V., Yao, Y.: On the finite-time blowup of a 1D model for the 3D axisymmetric Euler equations. arXiv preprint arXiv:1407.4776 (2014)

Choi, K., Kiselev, A., Yao, Y.: Finite time blow up for a 1D model of 2D Boussinesq system. Commun. Math. Phys. **334**(3), 1667–1679 (2015)

Constantin, P., Fefferman, C., Majda, A.J.: Geometric constraints on potentially singular solutions for the 3D Euler equations. Commun. Part. Differ. Equ. **21**, 3–4 (1996)

Deng, J., Hou, T.Y., Yu, X.: Geometric properties and nonblowup of 3D incompressible Euler flow. Commun. Part. Differ. Equ. **30**(1–2), 225–243 (2005)

Deng, J., Hou, T.Y., Yu, X.: Improved geometric conditions for non-blowup of the 3D incompressible Euler equation. Commun. Part. Differ. Equ. **31**(2), 293–306 (2006)

Escauriaza, L., Seregin, G.A., Sverak, V.: L3,∞-solutions of the Navier–Stokes equations and backward uniqueness. Russ. Math. Surv. **58**(2), 211 (2003)

Fefferman, C.L.: Existence and smoothness of the Navier–Stokes equation. Millenn. Prize Probl. 57–67 (2006)

Ferrari, A.B.: On the blow-up of solutions of the 3D Euler equations in a bounded domain. Commun. Math. Phys. **155**(2), 277–294 (1993)

Grauer, R., Sideris, T.C.: Numerical computation of 3D incompressible ideal fluids with swirl. Phys. Rev. Lett. **67**(25), 3511 (1991)

Hardy, G.H., Littlewood, J.E., Pólya, G.: Inequalities. Cambridge University Press, Cambridge (1952)

Hou, T.Y., Luo, G.: On the finite-time blowup of a 1D model for the 3D incompressible Euler equations. arXiv preprint arXiv:1311.2613 (2013)

Hou, T.Y., Shi, Z., Wang, S.: On singularity formation of a 3D model for incompressible Navier–Stokes equations. Adv. Math. **230**(2), 607–641 (2012)

Hou, T.Y., Lei, Z., Luo, G., Wang, S., Zou, C.: On finite time singularity and global regularity of an axisymmetric model for the 3D Euler equations. Arch. Ration. Mech. Anal. **212**(2), 683–706 (2014)

Hou, T.Y., Lei, Z.: On the stabilizing effect of convection in three-dimensional incompressible flows. Commun. Pure Appl. Math. **62**(4), 501–564 (2009)

Hou, T.Y., Li, R.: Dynamic depletion of vortex stretching and non-blowup of the 3D incompressible Euler equations. J. Nonlinear Sci. **16**(6), 639–664 (2006)

Hou, T.Y., Li, C.: Dynamic stability of the three-dimensional axisymmetric Navier–Stokes equations with swirl. Commun. Pure Appl. Math. **61**(5), 661–697 (2008)

Hou, T.Y., Liu, P.: Self-similar singularity of a 1D model for the 3D axisymmetric Euler equations. Res. Math. Sci. **2**(1), 1–26 (2015)

Kerr, R.M.: Evidence for a singularity of the three-dimensional, incompressible Euler equations. Phys. Fluids A Fluid Dyn. **5**(7), 1725–1746 (1993)

Klainerman, S., Majda, A.: Singular limits of quasilinear hyperbolic systems with large parameters and the incompressible limit of compressible fluids. Commun. Pure Appl. Math. **34**(4), 481–524 (1981)

Koch, H., Tataru, D.: Well-posedness for the Navier–Stokes equations. Adv. Math. **157**(1), 22–35 (2001)

Kozono, H., Taniuchi, Y.: Bilinear estimates in BMO and the Navier–Stokes equations. Math. Z. **235**(1), 173–194 (2000)

Landman, M.J., Papanicolaou, G.C., Sulem, C., Sulem, P.L.: Rate of blowup for solutions of the nonlinear Schrödinger equation at critical dimension. Phys. Rev. A **38**(8), 3837 (1988)

Landman, M., Papanicolaou, G.C., Sulem, C., Sulem, P.L., Wang, X.P.: Stability of isotropic self-similar dynamics for scalar-wave collapse. Phys. Rev. A **46**(12), 7869 (1992)

LeMesurier, B.J., Papanicolaou, G., Sulem, C., Sulem, P.L.: Focusing and multi-focusing solutions of the nonlinear Schrödinger equation. Phys. D Nonlinear Phenom. **31**(1), 78–102 (1988)

Liu, J.G., Wang, W.C.: Convergence analysis of the energy and helicity preserving scheme for axisymmetric flows. SIAM J. Numer. Anal. **44**(6), 2456–2480 (2006)

Luo, G., Hou, T.Y.: Toward the finite-time blowup of the 3D incompressible Euler equations: a numerical investigation. SIAM Multiscale Model. Simul. **12**(4), 1722–1776 (2014)

Majda, A.J., Bertozzi, A.L.: Vorticity and Incompressible Flow, vol. 27. Cambridge University Press, Cambridge (2002)

McLaughlin, D.W., Papanicolaou, G.C., Sulem, C., Sulem, P.L.: Focusing singularity of the cubic Schrödinger equation. Phys. Rev. A **34**(2), 1200 (1986)

Nirenberg, L.: On elliptic partial differential equations. Ann. Sc. Norm. Sup. Pisa. **13**, 115–162 (1959)

Papanicolaou, G.C., Sulem, C., Sulem, P.L., Wang, X.P.: The focusing singularity of the Davey–Stewartson equations for gravity–capillary surface waves. Phys. D Nonlinear Phenom. **72**(1), 61–86 (1994)

Prodi, G.: Un teorema di unicita per le equazioni di Navier–Stokes. Annali di Matematica pura ed applicata **48**(1), 173–182 (1959)

Pumir, A., Siggia, E.D.: Development of singular solutions to the axisymmetric Euler equations. Phys. Fluids A Fluid Dyn. (1989–1993) **4**(7), 1472–1491 (1992)

Sedov, L.I.: Similarity and Dimensional Methods in Mechanics. CRC Press, Boca Raton (1993)

Serrin, J.: The initial value problem for the Navier–Stokes equations. Nonlinear Probl. **9**, 69ff (1963)

Tao, T.: Structure and Randomness: Pages from Year one of a Mathematical Blog. American Mathematical Society, Providence (2008)

Tao, T.: Finite time blowup for an averaged three-dimensional Navier–Stokes equation. J. Am. Math. Soc. **29**(3), 601–674 (2016)

Weinan, E., Shu, C.W.: Small-scale structures in Boussinesq convection. Phys. Fluids **6**(1), 49–58 (1994)